

Optimized data collection and analysis process for studying solar-thermal desalination by machine learning

Guilong Peng^{#1,2}, Senshan Sun^{#2}, Yangjun Qin², Zhenwei Xu², Juxin Du², Swellam W. sharshir^{2,3}, A.W. Kandel^{2,3}, A.E. Kabeel^{2,4,5}, Nuo Yang^{*2}

¹School of Mechanical and Energy Engineering, Shaoyang University, Shaoyang 422000, China

²State Key Laboratory of Coal Combustion, Huazhong University of Science and Technology, Wuhan 430074, China

³Mechanical Engineering Department, Faculty of Engineering, Kafrelsheikh University, Kafrelsheikh 33516, Egypt

⁴Mechanical Power Engineering Department, Faculty of Engineering, Tanta University, Tanta, Egypt

⁵Faculty of Engineering, Delta University for Science and Technology, Gamasa, Egypt

#Guilong Peng and Senshan Sun contribute equally to this work

*Corresponding email: Nuo Yang (nuo@hust.edu.cn)

Abstract

An effective interdisciplinary study between machine learning and solar-thermal desalination requires a sufficiently large and well-analyzed experimental datasets. This study develops a modified dataset collection and analysis process for studying solar-thermal desalination by machine learning. Based on the optimized water condensation and collection process, the proposed experimental method collects over one thousand datasets, which is ten times more than the average number of datasets in previous works, by accelerating data collection and reducing the time by 83.3%. On the other hand, the effects of dataset features are investigated by using three different algorithms, including artificial neural networks, multiple linear regressions, and random forests. The investigation focuses on the effects of dataset size and range on prediction accuracy, factor importance ranking, and the model's generalization ability. The results demonstrate that a larger dataset can significantly improve prediction accuracy when using artificial neural networks and random forests. Additionally, the study highlights the significant impact of dataset size and range on ranking the importance of influence factors. Furthermore, the study reveals that the extrapolation data range significantly affects the extrapolation accuracy of artificial neural networks. Based on the results, massive dataset collection and analysis of dataset feature effects are important steps in an effective and consistent machine learning process flow for solar-thermal desalination, which can promote machine learning as a more general tool in the field of solar-thermal desalination.

Keywords: Solar desalination; Machine learning; Dataset collection; Production prediction; Artificial neural network.

Nomenclature

\hat{B}	List of regression coefficients	T_g	Glass cover temperature
c_1	Average values of productivity in $R_1(j)$ in RF	T_{ss}	Solar still types
c_2	Average values of productivity in $R_2(j)$ in RF	T_w	Water temperature
D	Normalized dataset	VIM_l^{DT}	Importance of one variable at node e in RF
e	Label of node	w	Weight between current layer and previous layer
E	Output error signal in BP-ANN	x	Input value
E_{min}	Threshold of root mean square error in BP-ANN	X	Array of experimental independent variables
f_i	Predicted value in ML	y	True productivity
H_F	Fan height above the basin	\bar{y}	Average productivity of datasets
GI	Gini impurity	y^{MLR}	Predicted value in MLR
h	Hyperparameters of BP-ANN	y^{neu}	Output of current neurons
i	Label of neurons in current layer in BP-ANN	y^{NN}	Predicted value in BP-ANN
j	Label of sample in RF	y^{RF}	Predicted value in RF
k	Number of independent variables	y_i	One of productivity
l	Label of neurons in previous layer in BP-ANN	Y	List of productivity
m	Number of neurons in current layer in BP-ANN	Greek letters	
M	label of regions in RF	α_q	Value of q_{th} neuron in first layer
\dot{m}	Productivity	β	Regression coefficient
m_t	Total mass of the collected freshwater increases with time	β_h	Value of h_{th} neuron in second layer
n	Number of DTs in RF	δ	relative prediction error
N	Sample size	$\bar{\delta}$	mean relative prediction error
N_M	Number of elements in region M in RF	δ^e	Error signal between current layer and previous layer
o_M	Average output value in DT	η	Scale coefficient
	Estimated probability that sample belongs to any class at node e in RF	Abbreviations	
\hat{p}_e		ANN	Artificial neural network
P_F	Power of the fan	BO	Bayesian optimization
q	Dimension label	BP-ANN	Backpropagation artificial neural network
$R(j)$	Regions sliced by j_{th} sample		Classification and regression trees
$R_M(j)$	Region of label M in RF	CART	
R_l	Random number	DT	Decision tree
R^2	Coefficient of determination	ML	Machine learning
Δt	Given period	MLR	Multiple linear regressions
T_{amb}	Ambient temperature	RF	Random forest
		STD	Solar-thermal desalination
		XPS	Extruded polystyrene

1. Introduction

The problem of safe drinking water is becoming increasingly serious due to the unbalanced distribution of water resources and environmental pollution, which leads to many problems, especially the health problems of residents in underdeveloped areas [1-3]. Seawater desalination technology plays an important role in solving this problem [4, 5]. Among the seawater desalination technologies, solar-thermal desalination (STD) has drawn much attention in the last decades, especially for small-scale and micro-scale systems, because of its simplicity, low investment cost, portability, and so on. [6-8]. On the other hand, machine learning (ML) methods have recently attracted much attention in many scientific fields, such as chemistry, physics, materials, biology, etc. [9, 10], because of their advantages of massive data analysis ability, saving of labor, economic costs, and time. The application of ML methods has been well studied in many solar energy fields, such as solar thermal collectors [11], solar cells [12-14], and solar radiation forecasting [15]. Therefore, an interdisciplinary study between ML and STD may have great potential, especially for analyzing a complex system with many influence factors that are difficult to be analyzed directly by the mathematical model.

Various algorithms have been applied to fit the results of STD systems in the past decades, including artificial neural networks (ANNs) [16-18], random forest (RF)[19, 20], hybrid fuzzy-neural algorithms [21], modified krill herd (MKH) algorithm [22], modified random vector functional link (RVFL) [23], and so on. For example, Noe et al. [24] found that up to 89% of the predictions were within 20% of actual production by using ANN based on 312 datasets. Mashaly et al. [25] developed a back propagation ANN model for the prediction of solar still performance, with a coefficient of determination (R^2) of 0.93 for predicting the productivity of seawater desalination. Later, they compared multi-layer perceptron neural networks and multiple linear regressions. The results showed that the average value of R^2 for the multi-layer perceptron model was higher by 11.23% than for the multiple linear

regressions model [26]. Recently, more efforts have been made to further optimize the conventional algorithms, such as developing the Imperialist Competition Algorithm enhanced ANN algorithm [27], optimizing ANN by using Harris Hawks Optimizer [28, 29] and Levenberg Marquardt algorithm [30, 31], and so on. The best-reported R^2 reaches up to near 1 [32-34].

Although the meaningful progress has been made in this cutting-edge topic, some important aspects cannot be deeply studied due to the limitation of the dataset size and dataset range of conventional experiments. Generally, conventional experimental setups require massive amounts of time to obtain only tens to a few hundred datasets [24, 35]. Such amount of data is insufficient, which not only impairs the model accuracy but also leads to an over-fitting problem and deteriorates the prediction capability. Meanwhile, the interdiscipline will be limited to a simple data fitting without further investigation, due to the insufficient dataset. On the other hand, it is difficult to directly collect large datasets from previously published works for analysis and comparison, due to the inconsistent measuring and analyzing standards [36]. In addition, the algorithms investigated in previous works were chosen empirically without strict consideration of the features of the datasets, hence the performance will be inconsistent by using the same algorithm. Thus, massive dataset collection and in-depth ML analysis remain big challenges in the interdiscipline between ML and STD.

The main objectives of this work are: (1) to explore an effective new method for speeding up and expanding the dataset collection of STD system, (2) then, to investigate the effect of important dataset features on ML analysis, such as size and range, and (3) finally, to propose an optimized standard process flow for analyzing STD systems by the ML method, which tries to eliminate the inconsistency of different works as much as possible, thus promoting ML as a more general tool in the field of STD.

In this work, firstly, a representative micro-scale STD system, i.e., the solar still system, was designed and optimized for collecting a large dataset of productivity, temperatures, and so on. Then, the effect of the dataset size on the prediction accuracy

of productivity was investigated. Meanwhile, the effect of the dataset range on the importance analysis of various influence factors was studied, such as water temperature, power of the fan, and so on. The model generalization performance was also discussed by extrapolating the production of different dataset ranges. Lastly, a standard process flow of analyzing STD systems by the ML method was proposed, which might promote the ML method to be a general tool of system analysis in the field of STD, along with theory, simulation, and so on.

2. Experiments and algorithms

Solar still, which is a typical small-scale STD system, is built as an example of investigating dataset collection and ML analysis. The solar still is a simple, low-cost, micro-scale STD system that requires minimal maintenance and has been extensively researched in recent decades [37-40]. The dataset collection involves three different types of solar stills: single-slope, double-slope, and pyramid. The basic working principle of a solar still is as follows: the seawater in the basin is heated by solar radiation and evaporates. The vapor rises due to natural or forced convection and condenses on the glass cover, which is cooler than the vapor. The condensate then slides down the glass cover by gravity and is collected in bottles. For more details on solar stills, please refer to [41, 42].

Based on the experimental setup (Fig.1a and 1b), six factors that influence the productivity (\dot{m}) of the solar still can be controlled and analyzed, namely: water temperature (T_w), glass cover temperature (T_g), ambient temperature (T_{amb}), power of the fan (P_F), fan height above the basin (H_F), solar still types (T_{ss}). T_w and T_g mainly depend on the heating power of the system. T_{amb} is regulated by a thermostat cover above the glass cover, which can vary from 10 °C to 35 °C. The validation of the thermostat cover can be found in our previous work [43]. A fan is mounted in the vapor chamber of the solar still. P_F and H_F can be changed to investigate the effect of air convection in the solar still. The bottom of the solar still measures 25 cm×25 cm and is insulated by a 4 cm layer of XPS (extruded polystyrene) foam. Besides, a

random number list, R_i , is also generated by the computer as a reference. The list of devices is shown in Table 1.

It is necessary to control each factor precisely for optimizing the experimental procedures and investigating the effect of each factor. Therefore, the stable artificial environment, instead of the real environment, is used in this work. Herein, electrical heating is used for simulating solar energy, which provides stable power input and shows the steady-state performance of the system [44]. The power density of electrical heating ranges from 0 W/m² to 1000 W/m². Besides, the ambient temperature is stably controlled by the thermostat cover as aforementioned.

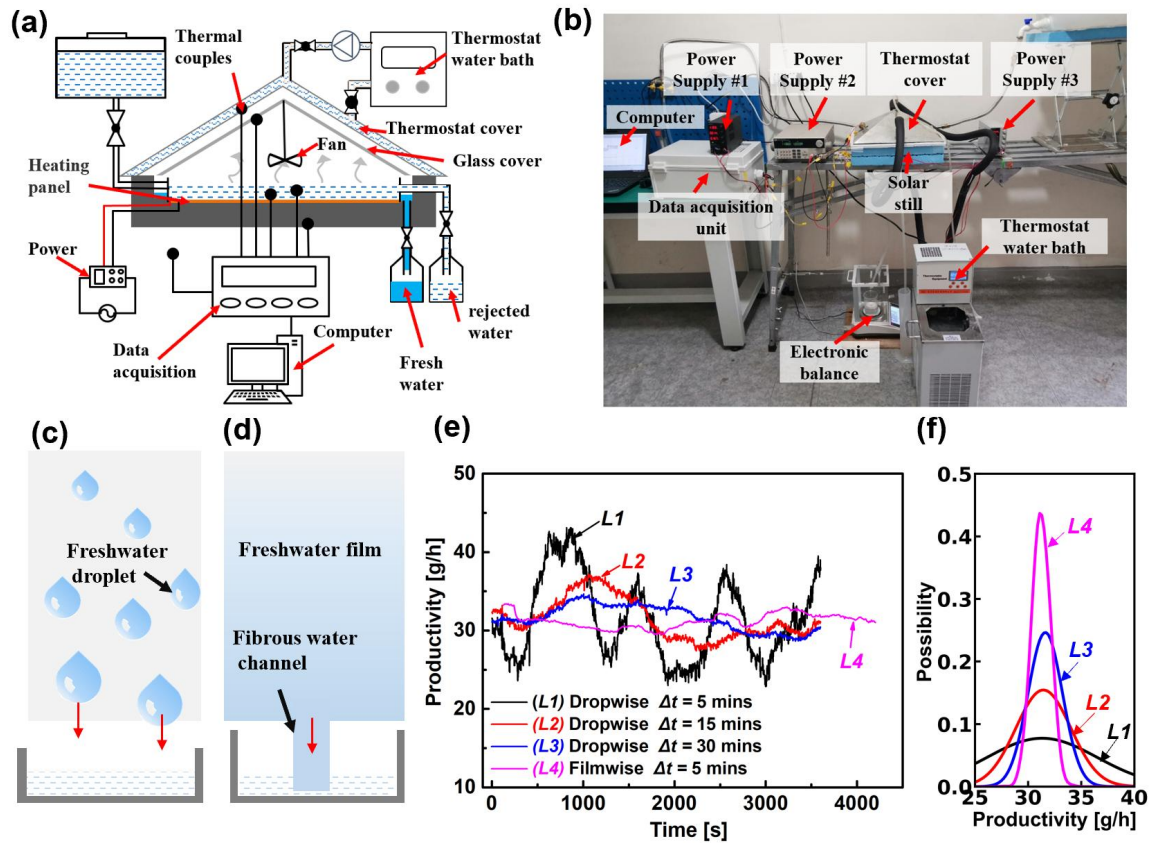


Fig.1 (a) Schematic diagram of the experimental setup (b) Photo of the experimental setup. (c) Collecting the drop-wise freshwater discretely. (d) Collecting the film-wise freshwater continuously. (e) Hourly productivity under different periods. (f) Standardized normal distribution of productivity.

In a conventional solar still system, the freshwater condenses as droplets as shown in Fig.1c. The total mass of the collected freshwater increases with time (m_t). The instantaneous freshwater productivity (\dot{m}) can be obtained from the freshwater

mass difference ($m_{t+\Delta t} - m_t = \Delta m$) during a given period (Δt), i.e., $\dot{m} = \Delta m / \Delta t$. However, Δm fluctuates with time, hence \dot{m} would be intrinsically unstable, especially under a small period as shown in Fig. 1e. When the period is 5 mins ($\Delta t = 5$ mins), the instantaneous productivity in conventional solar still ranges from 23 g/h to 43 g/h, although the thermal equilibrium state has been reached. The productivity fluctuates by 70% around the average value, thus completely unstable. For $\Delta t = 15$ mins, the productivity ranges from 27 g/h to 37 g/h, and the fluctuation remains as high as 18.5%. The fluctuation decreases to 10% when $\Delta t = 30$ mins. Therefore, in a conventional system, a long collecting time is inevitable to obtain just one single reliable dataset.

Table 1 Specifics of devices and sensors in the experiments.

Name	Brand	Type	Function	Range	Error
Fan	LFFAN	LFS0512SL	Enhancing convection	0 ~ 4800 RPM	10% RPM
Electronic balance	ANHENG	AH-A503	Measuring productivity	0 ~ 500 g	± 0.01 g
Power supply #1 & #3	WANPTEK	NPS3010W	DC power supply	0 ~ 30 V	± 0.1 %
Power supply #2	ITECH	IT6932A	Programmable power supply	0 ~ 60 V	± 0.03 %
Data acquisition unit	CAMPBELL	CR1000X&	Dataset collection	25 Channels	± 0.01 °C
	SCIENTIFIC	AM25T			
Thermostat water bath	QIWEI	DHC-2005-A	Controlling the ambient temperature	-20 ~ 99.9 °C	± 0.2 °C
Heating panel	BEISITE	Custom-made	Heating the water	0 ~ 2000 W/m ²	-
Thermal couple	ETA	T-K-36-SLE	Measuring the temperature	-200 ~ 260 °C	± 1.1 °C

After a careful evaluation of the data collection process, it is found that the unstable productivity of the conventional system resulted from the fluctuating falling frequency and size of freshwater droplets. To solve this problem, the glass cover is treated to be ultra-hydrophilic, which enables film condensation and avoids the droplets in previous works. In this work, anti-fog coating (Rain-X, Illinois tools works Inc.) is used for the treating process as an example. The condensate from the ultra-hydrophilic glass cover flows continuously to a bottle through a fibrous water

channel, as shown in Fig 1d. The weight of the collected condensate is recorded by the electronic balance every 10 seconds. After ultra-hydrophilic treatment, the instantaneous productivity ranges from 29.5 g/h to 33.5 g/h when $\Delta t = 5$ mins, which fluctuates by only 7%. It is even better than that of $\Delta t = 30$ mins in conventional solar still of previous works. Thus, the dataset collection time is saved by around 83.3% as compared to conventional systems. Fig. 1f compares the standardized normal productivity distribution of different conditions. The productivity of the proposed system (film-wise) at $\Delta t = 5$ mins is much more stable than that of the conventional system (drop-wise) even when its Δt is as long as 30 mins.

Due to the significantly reduced dataset collection time, much more datasets can be collected. Massive datasets are collected by changing the experimental condition. For example, datasets can be obtained automatically and continuously by changing the fan power (Fig. 2a). The stepwise fan power is controlled by the programable power supply. The corresponding productivity and temperatures in the stable state are recorded in the computer for further analysis. Then, one set of data that includes \dot{m} , T_w , T_g , T_{amb} , P_F , H_F , and T_{ss} is successfully obtained. In this work, 1022 datasets were collected for analysis, which is ten times more than the average number of datasets in previous works as shown in Fig. 2b.

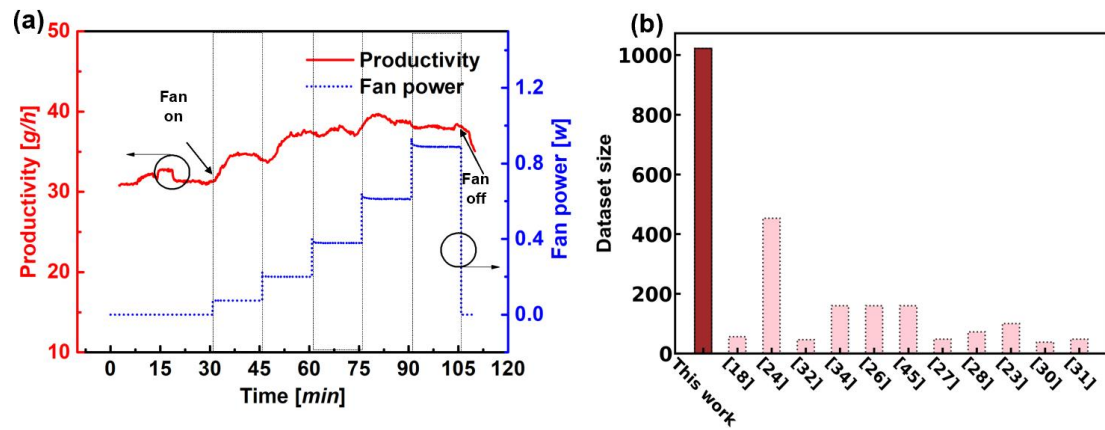


Fig. 2 (a) The productivity of solar still under stepped fan power. (b) Dataset size collected from the solar still in this work and the references.

To analyze the dataset from the solar still, three different algorithms were used and compared, including multiple linear regressions (MLR), backpropagation artificial neural network (BP-ANN), and random forest (RF).

(1) MLR model

MLR is a classic algorithm based on the least squares method that has been widely used in many fields for decades [45]. It has the advantages of speediness and convenience. MLR is derived through the utilization of the least squares method, which aims to minimize the sum of squared residuals. The equation for multiple linear regression can be expressed in matrix form as follows

$$y^{MLR} = \hat{\beta}_0 + \hat{\beta}_1 x_1 + \hat{\beta}_2 x_2 + \cdots + \hat{\beta}_k x_k \quad (1)$$

$$X^T X \hat{B} = X^T Y \quad (2)$$

where y^{MLR} is the predicted value, x is the input value, β is the regression coefficient. In the MLR model, the input dataset X is an array containing several experimental independent variables, such as T_w , T_g , T_{amb} , P_F , H_F , and T_{ss} . Y represents the list of productivity. The array \hat{B} represents the list of regression coefficients, which are determined through the fitting process using the dataset. Once \hat{B} has been fitted using the dataset, the productivity can be predicted using the MLR model. The detailed calculation processes can be found in “Supporting Information Note S3”.

(2) BP-ANN model

ANN is a popular neural algorithm in the field of STD due to its high accuracy [46]. ANN belongs to the black-box model, and the specific formulas cannot be obtained. The principle of ANN is similar to the information transmission of biological neurons. BP-ANN is a type of ANN in which the signal is forward propagated and the error is backpropagated. The model is continually revised through continuous error feedback. Then a high-precision predicting model is obtained. The variables in BP-ANN are the values of neurons in the input layer. In this work, the number of neurons in the input layer is 6, corresponding to 6 independent variables of experiments, which serve as the input features of the neural network. By calculating the values of neurons in the hidden layer with their corresponding weights, the final

result is obtained as the value of the output layer that has only one node. This value represents the predicted productivity based on the given independent variables and the BP-ANN model.

A five-layer perceptron with 3 hidden layers was used in this work. When a training sample is input, the output error signal E , of the BP-ANN model is

$$E = \frac{1}{2} (y^{NN} - y)^2 \quad (3)$$

where y^{NN} and y are the predicting and true values.

Utilizing the BP-ANN algorithm, the model propagates the error signal back through the network, and adjusts the weights between nodes, and the resulting updated outcome is represented as

$$w' = w + \Delta w = w - \frac{\partial E}{\partial w} \quad (4)$$

where w is the weight between the current layer and the previous layer according to the backpropagation. The activation function employed in this study is the unipolar sigmoid function. The weight adjustment is performed according to

$$\Delta w_{il} = \eta \delta_l^e y_i^{neu} \quad (5)$$

where i is the label of the neurons in the current layer, and l is the label of the neurons in the previous layer. y^{neu} is the output of the neuron using the activation function in the current layer; $\eta \in (0,1)$ is the scale coefficient, a larger η means a faster convergence speed but the local optimum may not be obtained, and a smaller η means higher accuracy and slower convergence speed. δ^e is the error signal between the current neural network layer and the previous layer, the results can be calculated by reverse iteration.

The bias can be represented

$$b' = b + \Delta b = b - \frac{\partial E}{\partial b}$$

Where b is the bias between the current layer and the previous layer according to the backpropagation. The biase is performed according to

$$\Delta b_j = \eta \sum_{i=1}^m \delta_j$$

For the training set with a sample size of N , the root mean square error is used as the total error of the model,

$$E_{RME} = \sqrt{\frac{1}{N} \sum_{i=1}^N \left[\frac{1}{2} (y_i^{NN} - y_i)^2 \right]} \quad (6)$$

When $E_{RME} < E_{min}$ is satisfied or the maximum number of iterations is reached, the training ends and the artificial neural network prediction model is obtained. The forward pass prediction process between the first and second layers is

$$\beta_h = AF \left[\sum_{i=1}^{m_1} (w_{ih}^2 x_i - b_h^1) \right] \quad h = 1, 2, \dots, m_2 \quad (7)$$

where m_1 is the number of neurons in the first layer, β_h is the value of the h_{th} neuron in the second layer, α_q is the value of the q_{th} neuron in the first layer. A similar process happens between the second and third layers, as shown in Fig. 3. All neurons are computed in the forward process, resulting in the final output. Please refer to the ‘‘Supplementary Information (Note S3)’’ for detailed calculation procedures.

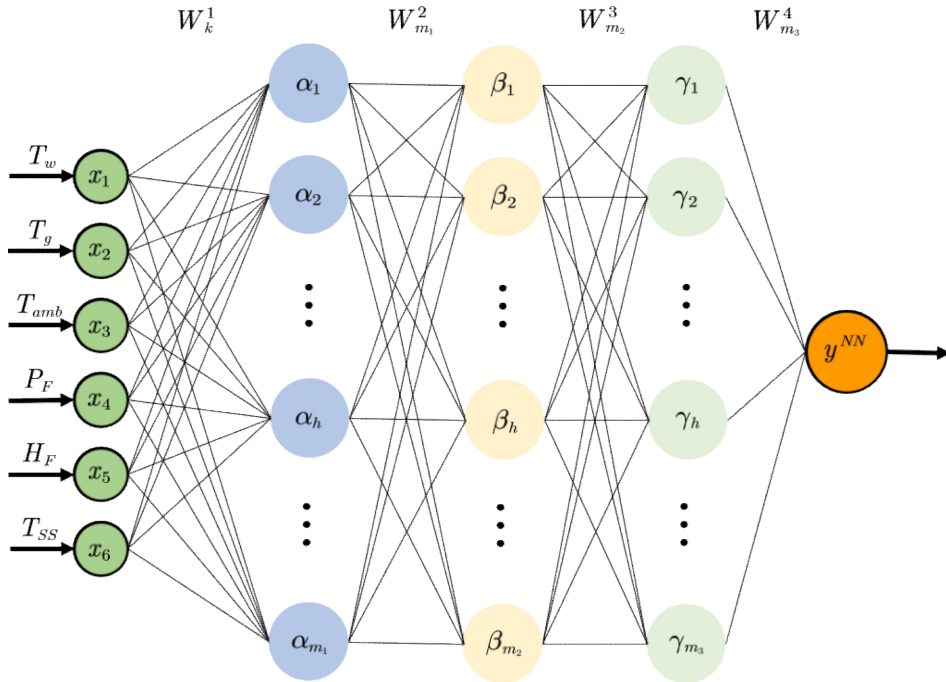


Fig. 3 Schematic diagram of BP-ANN algorithm.

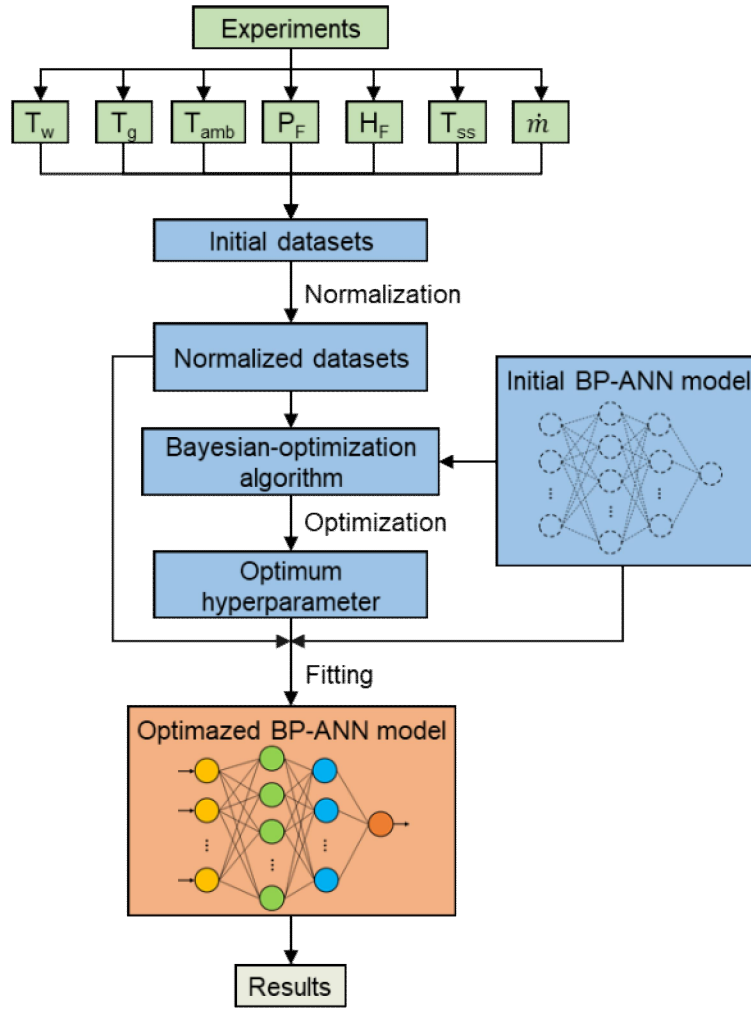


Fig. 4 The flow chart of using BP-ANN for productivity prediction of the STD system.

The overall flow chart of using BP-ANN for predicting the productivity of the STD system is shown in Fig. 4. The initial input consists of over 1000 experimental datasets that comprise six independent variables and one dependent variable, \dot{m} . To ensure consistent sample spacing, the initial dataset undergoes a data normalization process (Supporting Information Note S1). The initial BP-ANN model only consists of the BP-ANN algorithms, which are incapable of making predictions before training. Bayesian optimization (BO) is used for modifying the BP-ANN model to provide optimized hyperparameters, such as “hidden_layer_sizes”, “Activation” and “Solver”. For more details, please refer to the “Supporting Information Table S1”.

The BO process for BP-ANN is illustrated in Fig. 5. The optimization process for RF with BO is similar. The initial BP-ANN model and normalized datasets are inputted to construct the adjustment function as

$$R^2 = BPNN(h_1, h_2, h_3, h_4, h_5, D) \quad (8)$$

where R^2 is the coefficient of determination, $h_1 \sim h_5$ are the hyperparameters of BP-ANN, and D is the normalized dataset, which is constant in the fitting process.

The purpose of BO in this work is to find the optimum hyperparameters which can obtain the maximum R^2 . Firstly, the computer generates the random data points of the adjustment function within the defined domain. Based on the probabilistic surrogate model, the prediction function and confidence interval for the adjustment function are established. The acquisition function is employed to predict the quasi-optimal hyperparameters. If the threshold, defined as the maximum number of iterations in this work, is not met, the R^2 is calculated using the quasi-optimal hyperparameters. A new data point is generated based on this R^2 value and added to the existing data points of the adjustment function. The process is then repeated. Once the threshold is met, the quasi-optimal hyperparameters are considered the final optimum hyperparameters and are outputted. In this work, the probabilistic surrogate model is based on Gaussian process regression, while the acquisition function is based on the upper confidence bound. The detailed equations can be found in “Supporting Information Note S4”.

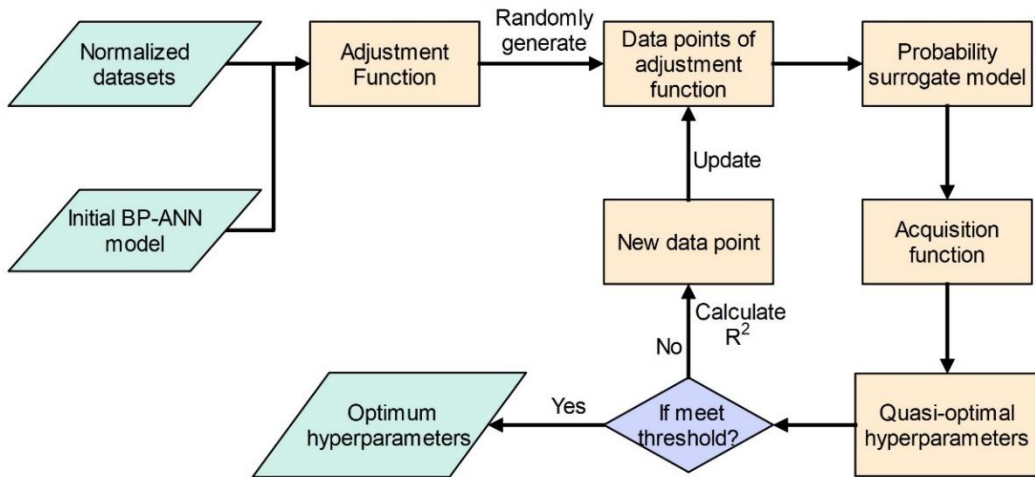


Fig. 5 Schematic diagram of the Bayesian optimization process.

(3) RF model

In recent years, the RF algorithm is one of the most popular algorithms and has

been widely used in Kaggle Competitions and academic dataset analysis [20]. RF is an ensemble learning method, which integrates multiple decision tree (DT) models. Based on the bagging, datasets are divided into numerous bootstrap samples to fit the DT models. The predicted result of RF is obtained by averaging the results of the DT models. The DT models of RF are independent of each other and can be calculated in parallel. Therefore, RF usually has a higher model training speed when dealing with large-scale datasets [47].

There are two main functions of RF for analyzing the STD system, including predicting the productivity and ranking the importance of influence factors:

a) Productivity prediction

RF is constructed by classification and regression trees (CART), which provides a flexible and powerful algorithm for regression tasks, offering interpretability, robustness, and handling of nonlinear relationships and mixed data types [48]. Utilizing the CART algorithm, a binary DT is constructed to partition each dimension into two regions. The output values are obtained within each region of the tree. Based on the heuristic algorithm, one sample, such as the j_{th} sample, will be chosen as the slicing variable and slicing point, which defines two regions, $R_1(j)$ and $R_2(j)$

$$R_1(j) = \{X_{jq}|y \leq y_j\} \quad R_2(j) = \{X_{jq}|y > y_j\} \quad (9)$$

where, q is the dimension label, which is an integer in the range $[1, k]$, and k is the number of the independent variables. X, y are the input variables. In this work, the input dataset X is an array containing experimental independent variables such as T_w , T_g , T_{amb} , P_F , H_F , and T_{ss} . y is the corresponding productivity, \dot{m} . The DT uses the principle of minimizing the squared error

$$MIN = \min_j \left[\min_{c_1} \sum_{x_i \in R_1(j)} (y_i - c_1)^2 + \min_{c_2} \sum_{x_i \in R_2(j)} (y_i - c_2)^2 \right] \quad (10)$$

where c_1 and c_2 are the average values of y in $R_1(j)$ and $R_2(j)$, respectively.

Traversing the variable j , the optimal segmentation point can be obtained for fixed input variables. Repeating the above process $N - 1$ times, the input space can be divided into N^k regions. The average output value, o_M , of each region is

$$o_M = \frac{1}{N_M} \sum_{y_j \in R_M(j)} y_i, \quad M = 1, 2, \dots, N^k \quad (11)$$

where M is the label of the regions; $R_M(j)$ is the region of label M ; N_M is the number of elements in the region M . The output of the decision tree model is

$$f(X_i) = o_M, \quad X_i \in R_M(j) \quad (12)$$

The output y^{RF} of the random forest model is

$$y^{RF} = F(X_i) = \frac{1}{n} \sum_{k=1}^n f_k(X_i) \quad (13)$$

where n is the number of DTs in the RF model.

After fitting the RF model, the prediction model $F(X_i)$ is obtained. If an input dataset X' is provided, the predicted productivity y' can be expressed as

$$y' = F(X') \quad (14)$$

b) Importance ranking

The quantitative importance of feature factors is calculated by using the Gini impurity. Based on the binary decision tree, the Gini impurity is

$$GI_e = 2\hat{p}_e(1 - \hat{p}_e) \quad (15)$$

where \hat{p}_e is the estimated probability that the sample belongs to any class at node e .

The importance of variable X_i at node e , VIM_{ie}^{DT} , that is, the change in Gini impurity before and after the branch of node e is

$$VIM_{ie}^{DT} = GI_e - GI_l - GI_r \quad (16)$$

where GI_l and GI_r is the Gini impurity of the two new nodes split by node e .

By calculating all the VIM_i^{DT} about variable X_i , the importance of the variable X_i in the random forest can be obtained. The specific calculation processes can be found in “Supplementary Information Note S3”. The overall flow chart of using RF for predicting productivity and calculating the factor importance of the STD system is similar to that of BP-ANN, as shown in “Supporting Information Fig. S1 and Fig. S2”.

To evaluate the prediction accuracy, three indicators were used in this work,

namely: relative prediction error (δ), mean relative prediction error ($\bar{\delta}$), and the coefficient of determination (R^2). The definitions are shown in Table 2. Where y_i is the experimental productivity of dataset i , f_i is the predicted productivity of dataset i , \bar{y} is the average productivity of all calculated datasets. Meanwhile, the calculation used the 5-fold cross-validation as discussed in “Supporting Information Note S5”. The fitting process with the optimum hyperparameter was performed 10 times with different training and testing datasets that were split randomly. The output evaluation indicators are the mean of these 10 results. Although this method may slightly reduce the accuracy of the fitted machine learning model, it avoids the overfitting problem and greatly enhances the generalization ability.

Table 2 The definitions of main evaluation indicators

Evaluation indicators	Expression
Relative prediction error (δ)	$\delta = \frac{y_i - f_i}{y_i} \times 100\%$
Mean relative prediction error ($\bar{\delta}$)	$\bar{\delta} = \frac{1}{n} \sum_{i=1}^n \delta$
Coefficient of determination (R^2)	$R^2 = 1 - \frac{\sum_{i=1}^n (y_i - f_i)^2}{\sum_{i=1}^n (y_i - \bar{y})^2}$

3. Results and discussions

Most previous works focused on using an algorithm to fit the experimental STD results accurately, without considering the dataset features, such as dataset size and range. However, the effects of dataset features are significant for choosing an algorithm in practical application, because different algorithms might require different dataset features. Moreover, investigating the effects of dataset features would help to understand the difference between various algorithms, which is useful to avoid the

inconsistency of different works. Therefore, the prediction performance of using BP-ANN, MLR, and RF based on different dataset features was investigated.

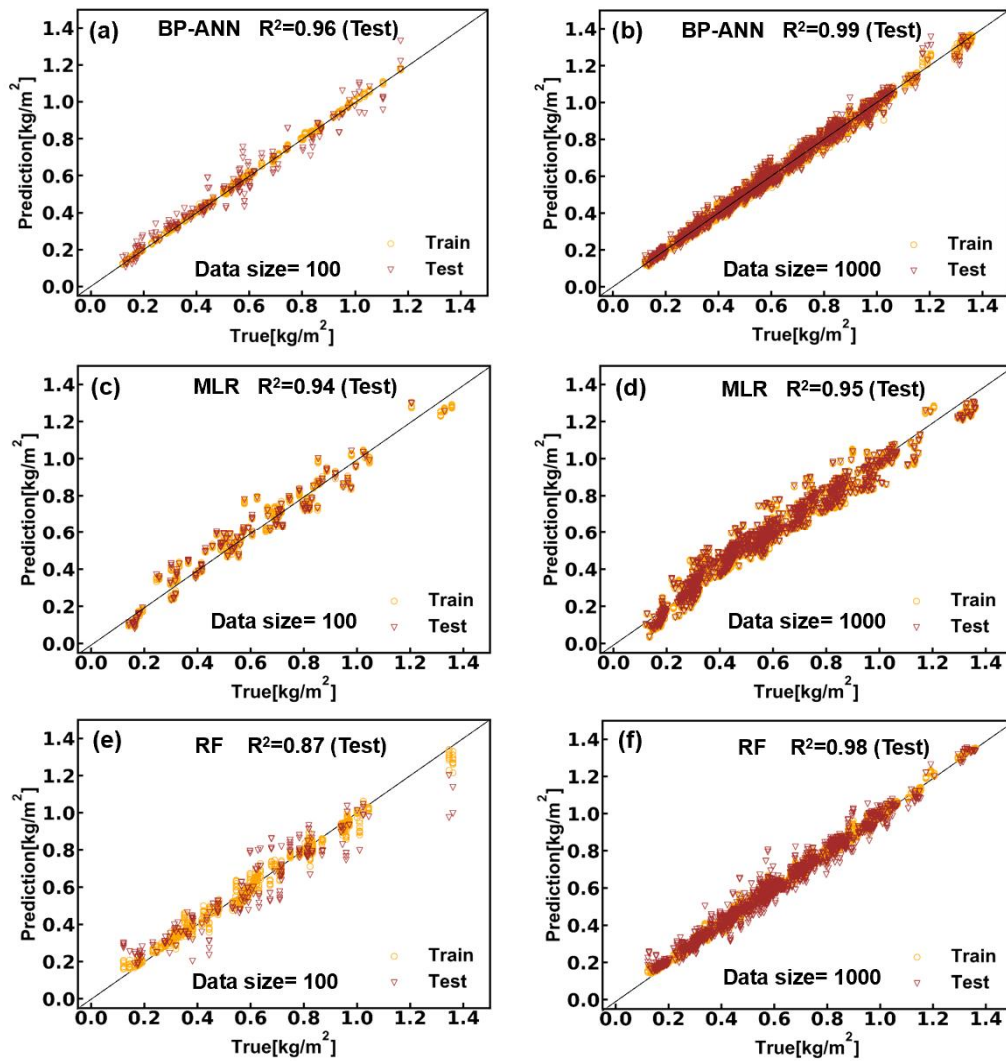


Fig. 6 Prediction and the true value of productivity by using (a) BP-ANN and 100 data points, (b)BP-ANN and 1000 data points, (c) MLR and 100 data points, and (d) MLR and 1000 data points, (e)RF and 100 data, (f) RF and 1000 data. The R^2 in the figure is the value of the testing set.

To investigate the effect of dataset size on the prediction of productivity, a series of datasets was randomly selected from the entire dataset. The R^2 of the testing set in BP-ANN is as high as 0.96 based on 100 datasets (Fig. 6a). The R^2 of the testing set increases from 0.96 to 0.99 when the dataset size increases from 100 to 1000, which indicates great predicting accuracy of BP-ANN under large dataset size (Fig. 6b). On the other hand, the R^2 of the testing set of MLR slightly increases from 0.94 to 0.95

when the dataset size increases from 100 to 1000 (Fig. 6c and 6d). The R^2 of RF shows the most significant improvement with the increases in the dataset size. The R^2 of the testing process is as low as 0.87 for 100 datasets and as high as 0.98 for 1000 dataset, which is comparable to BP-ANN. (Fig. 6e and 6f).

The R^2 of three algorithms under different dataset sizes are summarized in Fig. 7a. The R^2 of the training sets is almost constant for both BP-ANN and MLR but slightly increased for RF at first. On the other hand, the R^2 of the testing sets slightly increases with the dataset size for BP-ANN and MLR and dramatically increases for RF. In general, BP-ANN has a much better performance compared to MLR, regardless of the dataset size. However, between MLR and RF, superiority strongly depends on the dataset size. For the datasets of this work, RF will be better than MLR when the dataset size is more than 400. It's worth noting that, although BP-ANN outperforms RF in accuracy, the mean fitting time of BP-ANN is 5.9 times higher than that of RF. This is because RF consists of many independent decision trees, which can be computed in parallel, hence the increased computational speed. Therefore, given the training speed of BP-ANN and RF, RF might be a better choice when the dataset size is more than 1000.

In comparison to the clear trends of dataset size effect found in this work, the results collected from the references are quite inconsistent as shown in Fig. 7b. This is because different works have different optimization models, working conditions, analyzing standards, and so on, which makes it difficult to compare with each other. Therefore, a successful and comprehensive investigation of the STD system by ML relies on a consistent analysis and sufficient dataset, which is difficult to be obtained or concluded by collecting the results of current references. This emphasizes the importance of designing a rational experimental system for systematical dataset collection, as well as a standard process flow for ML analysis.

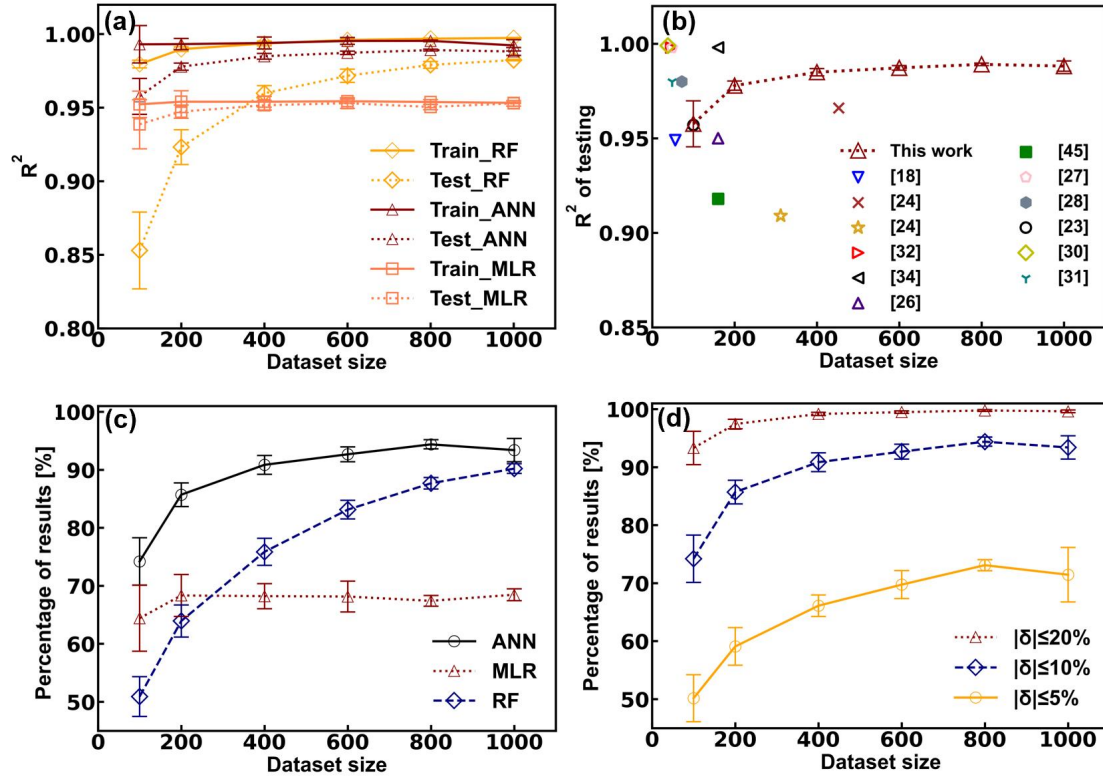


Fig. 7 The results of predicting the productivity of solar still by using different algorithms. (a) R^2 of the training sets and testing sets of BP-ANN, RF, and MLR based on different dataset sizes. (b) R^2 of the testing set of BP-ANN in various works. (c) Percentage of productivity in the testing sets for $|\delta| \leq 10\%$ by using BP-ANN, MLR, and RF. (d) Percentage of productivity in the testing sets for different ranges of δ by using BP-ANN.

Fig. 7c shows the percentage of predicted productivity that are within 10% of error, i.e., $|\delta| \leq 10\%$, by using BP-ANN, MLR, and RF. For BP-ANN, the percentages of δ within $\pm 10\%$ are 74.2%, 90.8%, and 93.4% for 100, 400, and 1000 datasets, respectively. Besides, 70% and 99.6% of the δ are less than $\pm 5\%$ and $\pm 20\%$, respectively, when the dataset size is more than 600 (Fig. 7d). In contrast, by using MLR, only 60% to 70% of the δ are less than $\pm 10\%$, even with a dataset size as high as 1000. On the other hand, for RF, as the dataset size increases from 100 to 1000, the percentage of results for δ within $\pm 10\%$ rises from 50.9% to 90.2%. This is comparable to BP-ANN when the dataset size reaches 1000, which is similar to the performance based on R^2 .

The results show that the performance of prediction might vary a lot although the dataset size only ranges from several hundreds to one thousand. Therefore, the choice

of the algorithm should take into account the dataset size and its effect on the accuracy, time cost, and other factors of each algorithm. Without a comprehensive consideration, previous studies with a small dataset size may suggest that BP-ANN outperforms RF, but the impact analysis of dataset size indicates that RF may be more time-effective when the dataset size exceeds one thousand. Thus, the interdisciplinary research of ML and STD should fully consider the influence of dataset size to reach more generalizable conclusions.

Secondly, besides the dataset size, the dataset range is another factor that affects the interdiscipline between ML and STD. Great dataset range indicates that the dataset covers all the possible conditions in practical applications, such as a wide water temperature or ambient temperature range. Herein, the factor importance, which could guide the system optimization by selecting the important factors of the desalination system for future optimization [19], is taken as an example of studying the effect of dataset range.

The factor importance is obtained by analyzing the connection between productivity and factors by using the RF algorithm. Fig. 8a shows the importance of T_w , T_g , T_{amb} , P_F , T_{ss} , and H_F in predicting productivity. The importance of the T_w , T_g , T_{amb} , P_F , and T_{ss} is relatively stable in different dataset sizes. This might be because the dataset range is the same for different dataset sizes. As aforementioned, different dataset sizes are obtained by randomly selecting a given amount of dataset from the entire dataset. Thus, every dataset covers almost all the experimental condition ranges, such as temperatures, fan powers, and so on. The difference is mainly the data density in each condition. On the contrary, the importance of the random list (R_L) decreases fast as the dataset size increases. R_L is a random list composed of 1, 2, and 3. The importance of R_L should be 0 in an ideal calculation. However, a subtle connection between R_L and productivity would exist when the dataset size is finite. The importance of H_F is similar to that of R_L , which indicates that H_F doesn't affect productivity. For small dataset sizes, such as 100, it is difficult to rank T_{ss} , H_F , and R_F reliably. Therefore, analyzing the factor importance with different dataset sizes could

help us to clearly distinguish the meaningful and meaningless factors, which is of great importance in complex systems with many influence factors.

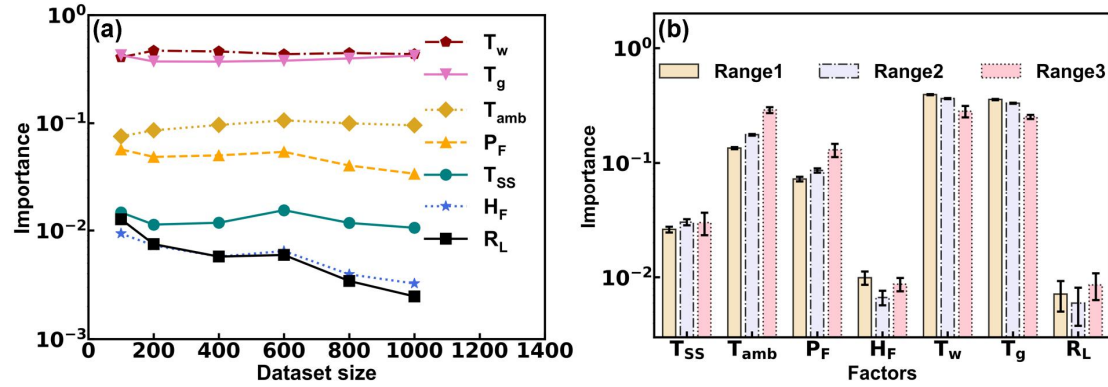


Fig. 8 The quantified importance of influence factor at different (a) dataset sizes, (b) ranges of T_w , Range 1 ($T_w = 30$ to 85°C), Range 2 ($T_w = 40$ to 75°C), and Range 3 ($T_w = 50$ to 65°C). R_L is a random list for comparison.

The effect of the water temperature range is investigated as an example of showing the effect of dataset range. Herein, three water temperature ranges are selected, including Range 1 ($T_w = 30$ to 85°C), Range 2 ($T_w = 40$ to 75°C), and Range 3 ($T_w = 50$ to 65°C). Fig. 8b shows the factor importance of different ranges. In the case of Range 1, the rank of importance is $T_w > T_g > T_{amb} > P_F > T_{ss} > H_F > R_L$. The importance of T_{amb} and P_F increases gradually and the importance of T_w and T_g decreases gradually as the range of T_w becomes more and more narrow. In the case of Range 3, T_{amb} becomes the most important factor, slightly higher than T_w and T_g . This means that if the possible range of an important factor is not completely measured, the importance of this factor will be significantly underestimated, while the importance of other factors will be overestimated. The effect of the data ergodicity from the aspect of P_F is shown in Supporting Information Fig. S4, which shows that the convergence range doesn't cover up or mislead the importance of the factors. Therefore, a great dataset range is quite important.

In addition, the effect of dataset range on the model generalization performance is investigated. The model generalization performance means the ability of the model

to extrapolate productivity, i.e., to predict the productivity of conditions that are beyond the existing experimental dataset range. Herein, the model generalization performance of BP-ANN is investigated due to its high accuracy among the three algorithms. The dataset is divided into 11 parts according to the range of T_w , as shown in Fig. 9a. Based on the range of T_w , four cases are investigated, namely “Case 1” to “Case 4”. In each case, 500 datasets are selected randomly for training and testing. For example, in “Case 1”, 500 datasets from range 2 to range 10 (yellow shadow) are selected for training and testing while the datasets in range 1 and range 11 (green rectangle) are used for prediction, which can validate the extrapolation model. In “Case 4”, 500 datasets from range 5 to range 7 are selected for training and testing, and the rest datasets are used for validating the extrapolation model. After training and testing, an ANN model is established, which can be used to calculate productivity in the extrapolation range. In this section, all the predicted datasets are out of the training and testing range, which demonstrates the model generalization performance.

To demonstrate the accuracy of extrapolation, the mean relative prediction error ($\bar{\delta}$) was calculated for all extrapolation ranges, as shown in Fig. 9b and Table 3. A low $\bar{\delta}$ indicates that most extrapolated productivities are close to the experimental productivities, hence a high extrapolation accuracy. The results show that a similar trend can be observed in all cases. $\bar{\delta}$ becomes larger when the predicted ranges are farther away from the edge of the training and testing dataset. Meanwhile, $\bar{\delta}$ increases more significantly in low water temperature compared to high water temperature. $\bar{\delta}$ is only around 4% to 5% when the predicted range is adjacent (0 - 5°C of difference) to the upper edge of training and testing sets. $\bar{\delta}$ remains as low as 9.1% even when the T_w in the predicting set is 20 to 25°C higher than the T_w in the training and testing set. On the contrary, $\bar{\delta}$ will be 8.6% to 13.2% for datasets adjacent to the lower edge of training and testing and larger than 15% when T_w is further away from the lower T_w edge of training and testing. In general, it can be inferred that BP-ANN might be used to predict the productivity of the unmeasured conditions that are adjacent to the measured conditions, but the accuracy might be different for near the upper edge and lower edge.

(a)

Range number	1	2	3	4	5	6	7	8	9	10	11
T_w [°C]	30-35	35-40	40-45	45-50	50-55	55-60	60-65	65-70	70-75	75-80	80-85
Case 1		500 data									
Case 2			500 data								
Case 3				500 data							
Case 4					500 data						
	Training and testing						Predicting				

(b)

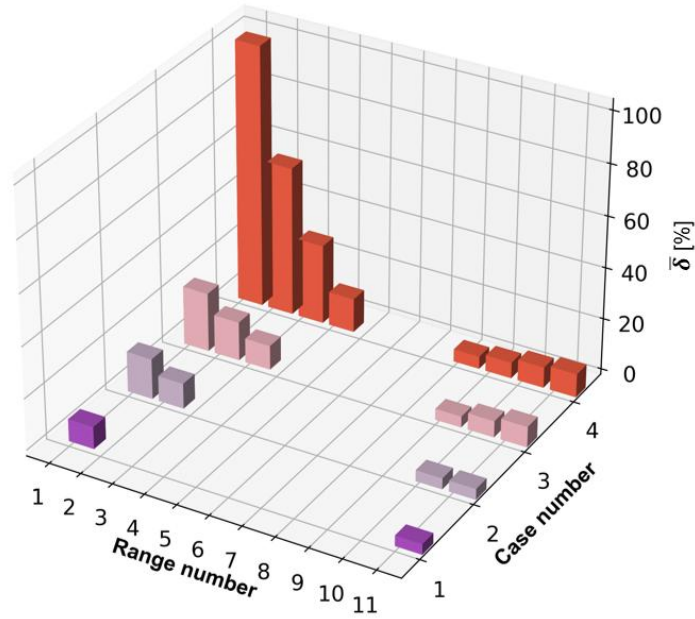


Fig.9 (a) Definition of cases and ranges. 500 Datasets are randomly selected for training and testing in each case. (b)The average relative error ($\bar{\delta}$) of productivity extrapolation under different ranges of T_w (Case 1 to Case 4).

Table 3 $\bar{\delta}$ of productivity extrapolation for different cases.

Range number	1 (30-35°C)	2 (35-40°C)	3 (40-45°C)	4 (45-50°C)	8 (65-70°C)	9 (70-75°C)	10 (75-80°C)	11 (80-85°C)
Case 1	$8.6 \pm 0.8\%$	-	-	-	-	-	-	$4.0 \pm 0.5\%$
Case 2	$15.7 \pm 2.2\%$	$9.8 \pm 0.7\%$	-	-	-	-	$4.2 \pm 0.5\%$	$4.2 \pm 1.2\%$
Case 3	$22.8 \pm 2.8\%$	$15.1 \pm 2.3\%$	$9.4 \pm 1.1\%$	-	-	$4.3 \pm 0.2\%$	$6.3 \pm 0.7\%$	$8.0 \pm 1.1\%$
Case 4	$102.1 \pm 42.5\%$	$58.1 \pm 25.5\%$	$30.9 \pm 10.6\%$	$13.2 \pm 3.5\%$	$4.9 \pm 0.3\%$	$6.2 \pm 0.7\%$	$8.0 \pm 2.0\%$	$9.1 \pm 5.2\%$

4. A standard process flow of interdisciplinary study

This work shows that dataset features have significant effects on the interdisciplinary between ML and STD, which were overlooked in previous works. Therefore, dataset features should be taken into account in the whole process of interdisciplinary study, making the process more general and standard, which is crucial for promoting ML to be a general tool for optimizing and analyzing STD. Fig.10 illustrates the modified standard process flow of the interdisciplinary study proposed by this work. In addition to some common steps in conventional studies, two key processes are suggested based on the results of this work.

Fig.10 Proposed standard process flow for the interdisciplinary study between machine learning and solar-thermal desalination. The suggested new process flow will enable a more effective, reliable, and standardized analysis, compared to the process flow in previous studies.

The proposed standard process flow consists of seven processes:

- (3) The datasets, obtained from the designed STD platform, are preprocessed, such as normalization, shuffle, removal of invalid datasets, and so on.
- (4) Algorithm selection, which is based on the purpose of the study and the characteristic of datasets.
- (5) The algorithm should be optimized by using optimizers for choosing proper hyperparameters, such as “max_depth”, “max_features”, and “n_estimators” in RF. The optimizers include Bayesian, genetic algorithm, Harris Hawks Optimizer, etc.
- (6) Importantly, independence verification of dataset features should be carried out, which is missing in previous studies on STD systems. To select the best algorithm and give a consistent result, the dependence of dataset features, such as size, range, factors, etc. should be checked carefully. In the review of previous works, there are some inconsistent conclusions, partially due to missing the step of independence verification. It is easier to obtain valuable and universal conclusions with independence verification. For example, it is more confident to claim that BP-ANN is better than MLR after dataset size independence verification.
- (7) Finally, the desired results are outputted.

5. Conclusion

This study first investigated the dataset collection of a typical solar thermal desalination system. To obtain a large dataset, the experimental setup of solar-thermal desalination was optimized by collecting freshwater via film-wise condensation. This reduced dataset collection time by 83.3% compared to conventional systems. The study collected 1022 datasets, each dataset included productivity, water temperature, glass temperature, fan power, fan height above the basin, and types of solar stills.

Secondly, the effect of dataset features on machine learning analysis was studied based on the collected datasets, including the effect of dataset size and range on productivity prediction, factor importance analysis, and productivity extrapolation.

The results demonstrate that dataset size significantly affects productivity prediction. 93.4% and 90.2% of relative prediction errors are less than $\pm 10\%$ for the artificial neural network and random forest algorithms by 1000 datasets, and 74.2%, 50.9% by 100 datasets, respectively. In contrast, multiple linear regression remained at a low percentage across all dataset sizes. Furthermore, sufficient dataset size helps to distinguish meaningful and meaningless factors. On the other hand, ensuring a sufficient dataset range is also crucial for accurately ranking influence factors. The study also found that extrapolating productivity via the artificial neural network was possible when the extrapolating dataset range is adjacent to the training and testing dataset range. In addition, extrapolating productivity for high temperatures is found more accurate than for low water temperatures.

Finally, this work proposed a new standard interdisciplinary process flow to promote the use of machine learning as a general tool in solar-thermal desalination. The standard process flow comprises seven subprocesses, including the determination of purpose, the establishment of a quick and massive data collection platform, dataset preprocessing, algorithm selection, algorithm optimization, independence validation, and results output.

In summary, this study represents a meaningful step towards more in-depth interdisciplinary research between machine learning and solar-thermal desalination.

6. Conflicts of interest

There are no conflicts of interest to declare.

7. Acknowledgment

The work was sponsored by the National Key Research and Development Program of China (2018YFE0127800) and Fundamental Research Funds for the Central Universities (2019kfyRCPY045). The authors thank the National Supercomputing Center in Tianjin (NSCC-TJ) and China Scientific Computing Grid (ScGrid) for assisting in computations.

8. References

- [1] Shannon MA, Bohn PW, Elimelech M, Georgiadis JG, Marinas BJ, Mayes AM. Science and technology for water purification in the coming decades. *Nature*. 2008;452:301-10.
- [2] Lord J, Thomas A, Treat N, Forkin M, Bain R, Dulac P, et al. Global potential for harvesting drinking water from air using solar energy. *Nature*. 2021;598:611-7.
- [3] Ray I, Smith KR. Towards safe drinking water and clean cooking for all. *The Lancet Global Health*. 2021;9:e361-e5.
- [4] Elimelech M, Phillip WA. The Future of Seawater Desalination: Energy, Technology, and the Environment. *Science*. 2011;333:712-7.
- [5] Chowdhury MR, Steffes J, Huey BD, McCutcheon JR. 3D printed polyamide membranes for desalination. *Science*. 2018;361:682-6.
- [6] Wang Z, Horseman T, Straub AP, Yip NY, Li D, Elimelech M, et al. Pathways and challenges for efficient solar-thermal desalination. *Sci Adv*. 2019;5:eaax0763.
- [7] Menon AK, Haechler I, Kaur S, Lubner S, Prasher RS. Enhanced solar evaporation using a photo-thermal umbrella for wastewater management. *Nat Sustainability*. 2020;3:144-51.
- [8] Li J, Wang X, Lin Z, Xu N, Li X, Liang J, et al. Over 10 kg m⁻² h⁻¹ Evaporation Rate Enabled by a 3D Interconnected Porous Carbon Foam. *Joule*. 2020;4:1-10.
- [9] Butler KT, Davies DW, Cartwright H, Isayev O, Walsh A. Machine learning for molecular and materials science. *Nature*. 2018;559:547-55.
- [10] Jumper J, Evans R, Pritzel A, Green T, Figurnov M, Ronneberger O, et al. Highly accurate protein structure prediction with AlphaFold. *Nature*. 2021;596:583-9.
- [11] Osorio JD, Wang Z, Karniadakis G, Cai S, Chrysostomidis C, Panwar M, et al. Forecasting solar-thermal systems performance under transient operation using a data-driven machine learning approach based on the deep operator network architecture. *Energy Convers Manage*. 2022;252:115063.
- [12] Mahmood A, Wang J-L. Machine learning for high performance organic solar cells: current scenario and future prospects. *Energy Environ Sci*.

2021;14:90-105.

- [13] Odabaşı Ç, Yıldırım R. Performance analysis of perovskite solar cells in 2013 – 2018 using machine-learning tools. *Nano Energy*. 2019;56:770-91.
- [14] Sahu H, Rao W, Troisi A, Ma H. Toward predicting efficiency of organic solar cells via machine learning and improved descriptors. *Adv Energy Mater*. 2018;8:1801032.
- [15] Voyant C, Notton G, Kalogirou S, Nivet M-L, Paoli C, Motte F, et al. Machine learning methods for solar radiation forecasting: A review. *Renewable Energy*. 2017;105:569-82.
- [16] Mashaly AF, Alazba AA. Comparison of ANN, MVR, and SWR models for computing thermal efficiency of a solar still. *Int J Green Energy*. 2016;13:1016-25.
- [17] Sohani A, Hoseinzadeh S, Samiezadeh S, Verhaert I. Machine learning prediction approach for dynamic performance modeling of an enhanced solar still desalination system. *J Therm Anal Calorim*. 2022;147:3919-30.
- [18] Mashaly AF, Alazba AA. Thermal performance analysis of an inclined passive solar still using agricultural drainage water and artificial neural network in arid climate. *Sol Energy*. 2017;153:383-95.
- [19] Wang Y, Peng G, Sharshir SW, K AW, eal e, Yang N. The Weighted Values of Solar Evaporation's Environment Factors Obtained by Machine Learning. *ES Materials & Manufacturing*. 2021;14:87-94.
- [20] Gao W, Shen L, Sun S, Peng G, Shen Z, Wang Y, et al. Forecasting solar still performance from conventional weather data variation by machine learning method. *Chin Phys B*. 2023;32:048801.
- [21] Rezvani A, Gandomkar M. Modeling and control of grid connected intelligent hybrid photovoltaic system using new hybrid fuzzy-neural method. *Sol Energy*. 2016;127:1-18.
- [22] Chen W, Shao Z, Wakil K, Aljojo N, Samad S, Rezvani A. An efficient day-ahead cost-based generation scheduling of a multi-supply microgrid using a modified krill herd algorithm. *J Cleaner Prod*. 2020;272:122364.

- [23] Sharshir SW, Abd Elaziz M, Elkadeem MR. Enhancing thermal performance and modeling prediction of developed pyramid solar still utilizing a modified random vector functional link. *Sol Energy*. 2020;198:399-409.
- [24] Santos NI, Said AM, James DE, Venkatesh NH. Modeling solar still production using local weather data and artificial neural networks. *Renewable Energy*. 2012;40:71-9.
- [25] Mashaly AF, Alazba AA, Al-Awaadh AM, Mattar MA. Predictive model for assessing and optimizing solar still performance using artificial neural network under hyper arid environment. *Sol Energy*. 2015;118:41-58.
- [26] Mashaly AF, Alazba AA. MLP and MLR models for instantaneous thermal efficiency prediction of solar still under hyper-arid environment. *Comput Electron Agric*. 2016;122:146-55.
- [27] Nazari S, Bahiraei M, Moayedi H, Safarzadeh H. A proper model to predict energy efficiency, exergy efficiency, and water productivity of a solar still via optimized neural network. *J Cleaner Prod*. 2020;277:123232.
- [28] Essa FA, Abd Elaziz M, Elsheikh AH. An enhanced productivity prediction model of active solar still using artificial neural network and Harris Hawks optimizer. *Appl Therm Eng*. 2020;170:115020.
- [29] Pavithra S, Veeramani T, Subha SS, Kumar PS, Shanmugan S, Elsheikh AH, et al. Revealing prediction of perched cum off-centered wick solar still performance using network based on optimizer algorithm. *Process Safety and Environmental Protection*. 2022;161:188-200.
- [30] Dumka P, Chauhan R, Mishra DR. Experimental and theoretical evaluation of a conventional solar still augmented with jute covered plastic balls. *J Storage Mater*. 2020;32:101874.
- [31] Chauhan R, Dumka P, Mishra DR. Modelling conventional and solar earth still by using the LM algorithm-based artificial neural network. *Int J Ambient Energy*. 2020;43:1389-96.
- [32] Hamdan MA, Khalil RAH, Abdelhafez EAM. Comparison of Neural Network Models in the Estimation of the Performance of Solar Still Under Jordanian

- Climate. *Journal of Clean Energy Technologies*. 2014;238-42.
- [33] Maddah HA, Bassyouni M, Abdel-Aziz MH, Zoromba MS, Al-Hossainy AF. Performance estimation of a mini-passive solar still via machine learning. *Renewable Energy*. 2020;162:489-503.
- [34] Alazba AA, Mashaly AF. Comparative investigation of artificial neural network learning algorithms for modeling solar still production. *Journal of Water Reuse and Desalination*. 2015;5:480-93.
- [35] Wang Y, Kandeal A, Swidan A, Sharshir SW, Abdelaziz GB, Halim M, et al. Prediction of tubular solar still performance by machine learning integrated with Bayesian optimization algorithm. *Appl Therm Eng*. 2021;184:116233.
- [36] Rashidi S, Karimi N, Yan W-M. Applications of machine learning techniques in performance evaluation of solar desalination systems – A concise review. *Eng Anal Boundary Elem*. 2022;144:399-408.
- [37] Ni G, Zandavi SH, Javid SM, Boriskina SV, Cooper TA, Chen G. A salt-rejecting floating solar still for low-cost desalination. *Energy Environ Sci*. 2018;11:1510-9.
- [38] Xu Z, Zhang L, Zhao L, Li B, Bhatia B, Wang C, et al. Ultrahigh-efficiency desalination via a thermally-localized multistage solar still. *Energy Environ Sci*. 2020;13:830-9.
- [39] Katekar VP, Deshmukh SS. A review on research trends in solar still designs for domestic and industrial applications. *J Cleaner Prod*. 2020;257:120544.
- [40] Peng G, Sharshir SW, Wang Y, An M, Ma D, Zang J, et al. Potential and challenges of improving solar still by micro/nano-particles and porous materials - A review. *J Cleaner Prod*. 2021;311:127432.
- [41] Peng G, Sharshir SW, Hu Z, Ji R, Ma J, Kabeel AE, et al. A compact flat solar still with high performance. *Int J Heat Mass Transfer*. 2021;179:121657.
- [42] Sharshir SW, Yang N, Peng G, Kabeel AE. Factors affecting solar stills productivity and improvement techniques: A detailed review. *Appl Therm Eng*. 2016;100:267-84.
- [43] Peng G, Xu Z, Ji J, Sun S, Yang N. A study on the upper limit efficiency of solar

still by optimizing the mass transfer. *Appl Therm Eng.* 2022;118664.

- [44] Chen Z, Yao Y, Zheng Z, Zheng H, Yang Y, Hou La, et al. Analysis of the characteristics of heat and mass transfer of a three-effect tubular solar still and experimental research. *Desalination.* 2013;330:42-8.
- [45] Mashaly AF, Alazba AA. Experimental and modeling study to estimate the productivity of inclined passive solar still using ANN methodology in arid conditions. *J Water Supply Res Technol AQUA.* 2018;67:332-46.
- [46] He Q, Zheng H, Ma X, Wang L, Kong H, Zhu Z. Artificial intelligence application in a renewable energy-driven desalination system: A critical review. *Energy and AI.* 2022;7:100123.
- [47] Mishina Y, Murata R, Yamauchi Y, Yamashita T, Fujiyoshi H. Boosted Random Forest. *IEICE Trans Inf Syst.* 2015;E98.D:1630-6.
- [48] Breiman L. Random forests. *Machine learning.* 2001;45:5-32.

Supporting Information

Optimized data collection and analysis process for studying solar-thermal desalination by machine learning

Guilong Peng^{#1,2}, Senshan Sun^{#2}, Yangjun Qin², Zhenwei Xu², Juxin Du², Swellam W. sharshir^{2,3}, A.W. Kandel^{2,3}, A.E. Kabeel^{2,4,5}, Nuo Yang^{*2}

¹School of Mechanical and Energy Engineering, Shaoyang University, Shaoyang 422000, China

²State Key Laboratory of Coal Combustion, Huazhong University of Science and Technology, Wuhan 430074, China

³Mechanical Engineering Department, Faculty of Engineering, Kafrelsheikh University, Kafrelsheikh 33516, Egypt

⁴Mechanical Power Engineering Department, Faculty of Engineering, Tanta University, Tanta, Egypt

⁵Faculty of Engineering, Delta University for Science and Technology, Gamasa, Egypt

*Corresponding email: Nuo Yang (nuo@hust.edu.cn)

Note S1、 The process of data standardization

The accuracy of the model suffers because data attributes with larger magnitudes dominate. In this work, the Z-Scale normalization method is used to normalize the data. The Z-Scale method is based on the mean and standard deviation of the original data and keeps the sample spacing formula as

$$x'_i = \frac{x_i - \mu}{\delta} \quad (S1)$$

where x'_i is the value after normalization; x_i is the original value; μ is the mean value; δ is the population standard deviation.

The Python library “sklearn.preprocessing” is used in this part.

Note S2、 The method of splitting the data set

The data is split into training and test sets. The training set is used to train the model, and the test set is used to test the training results of the model. Generally, 20% of the data is used as the test set ^[1]. The Python library “sklearn.model_selection” is used in this part.

Note S3、 The process of training model

Random forest model (RF), backpropagation neural network model (BP-ANN), and multiple linear regression model (MLR) are built in this part.

3.1 RF

Firstly, let the input variable be X, Y

$$X = \begin{pmatrix} X_1 \\ X_2 \\ \vdots \\ X_N \end{pmatrix} = \begin{pmatrix} x_{1\ 1} & x_{1\ 2} & \cdots & x_{1\ k} \\ x_{2\ 1} & x_{2\ 2} & \cdots & x_{2\ k} \\ \vdots & \vdots & \ddots & \vdots \\ x_{N\ 1} & x_{N\ 2} & \cdots & x_{N\ k} \end{pmatrix}, \quad Y = \begin{pmatrix} y_1 \\ y_2 \\ \vdots \\ y_N \end{pmatrix} \quad (S2)$$

where N is the sample volume of the training set, and k is the number of feature parameters. There is a training set D .

$$D = \begin{pmatrix} D_1 \\ D_2 \\ \vdots \\ D_N \end{pmatrix} = \begin{pmatrix} x_{1\ 1} & x_{1\ 2} & \cdots & x_{1\ k} & y_1 \\ x_{2\ 1} & x_{2\ 2} & \cdots & x_{2\ k} & y_2 \\ \vdots & \vdots & \ddots & \vdots & \vdots \\ x_{N\ 1} & x_{N\ 2} & \cdots & x_{N\ k} & y_N \end{pmatrix} \quad (S3)$$

Based on the classification and regression trees (CART) algorithm, a binary decision tree is built to divide each dimension into two regions, and the output values are got in each region. Based on the heuristic algorithm, the j th samples are chosen as the slicing variable and slicing point, which defines two regions.

$$R_1(j) = \{X_{j\ q}|y \leq y_j\} \quad R_2(j) = \{X_{j\ q}|y > y_j\} \quad (S4)$$

where, q is the dimension label, which is an integer in the range $[1, k]$.

The decision tree uses the principle of minimizing the squared error

$$MIN = \min_j \left[\min_{c_1} \sum_{x_i \in R_1(j)} (y_i - c_1)^2 + \min_{c_2} \sum_{x_i \in R_2(j)} (y_i - c_2)^2 \right] \quad (S5)$$

where

$$\hat{c}_1 = \frac{1}{N_1} \sum_{X_{i\ q} \in R_1(j)} y_i, \quad \hat{c}_2 = \frac{1}{N_2} \sum_{X_{i\ q} \in R_2(j)} y_i \quad (S6)$$

where the N_1, N_2 are the number of elements in $R_1(j)$ and $R_2(j)$, respectively.

Traversing the variable j , for a fixed input variable $D_{j\ q}$, the optimal segmentation point s can be obtained.

Repeating the above process $N - 1$ times, the input space can be divided into N^k regions and the output value corresponding to each region is

$$o_M = \frac{1}{N_M} \sum_{y_j \in R_M(j)} y_i, \quad M = 1, 2, \dots, N^k \quad (S7)$$

where M is the label of the regions; $R_M(j)$ is the region of label M ; N_M is the number of elements in the region M .

The output of the decision tree model is

$$f(X_i) = o_M, \quad X_i \in R_M(j) \quad (S8)$$

The output of the random forest model is

$$F(X_i) = \frac{1}{n} \sum_{k=1}^n f_k(X_i) \quad (S9)$$

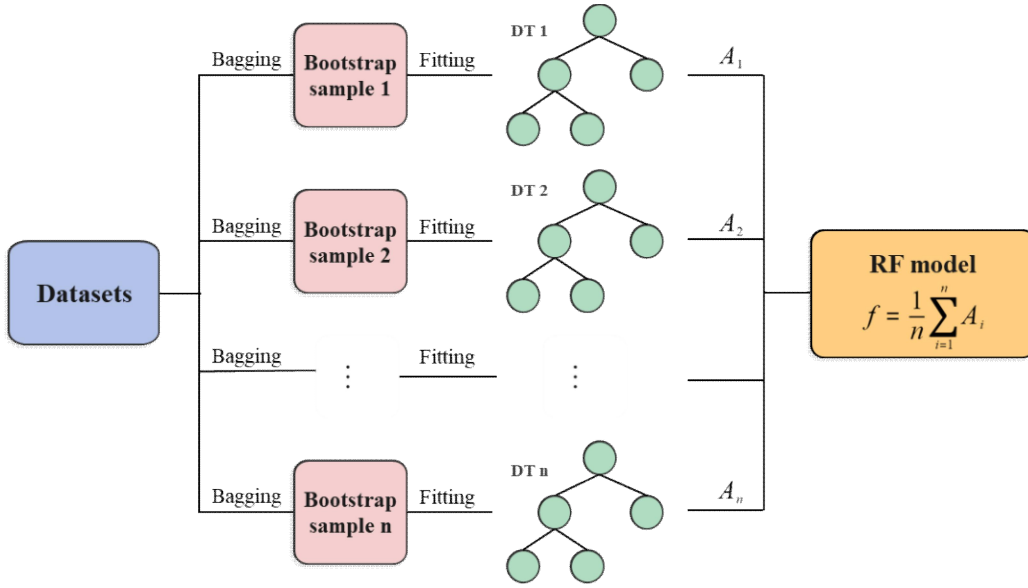


Fig. S1 Schematic diagram of RF algorithm

The influence of feature parameters is calculated by using the Gini impurity. Based on the binary decision tree, the Gini impurity is

$$GI_e = 2\hat{p}_e(1 - \hat{p}_e) \quad (S10)$$

where \hat{p}_e is the estimated probability that the sample belongs to any class at node e .

The influence of variable Q_i at node e , that is, the change in Gini impurity before and after the branch of node e is

$$VIM_{ie}^{DT} = GI_e - GI_l - GI_r \quad (S11)$$

where GI_l and GI_r is the Gini impurity of the two new nodes split by node e .

If the variable Q_i appears E times in the decision tree, the influence of the variable Q_i in the decision tree is

$$VIM_i^{DT} = \sum_{e=1}^E VIM_{ie}^{DT} \quad (S12)$$

The influence of variable Q_i in the random forest is

$$VIM_i^{RF} = \frac{1}{n} \sum_{j=1}^n VIM_{ij}^{DT} \quad (S13)$$

where n is the number of the decision trees in the random forest.

The flow chart of using RF for predicting productivity and calculating the factor importance of the STD system is shown in Fig.S2. The initial input consists of over 1000 experimental dataset that comprises seven factors. To ensure consistent sample

spacing, the initial dataset undergoes a data normalization process. The initial Random Forest (iRF) model only consists of the Random Forest algorithms. Before fitting the model with the dataset, the iRF does not possess the capability to make predictions. The Bayesian optimization (BO) algorithm is employed to determine the optimum hyperparameters by combining the iRF and the normalized dataset. There are data training and testing processes during BO based on iRF. The BO modified model is obtained by fitting the iRF with the optimum hyperparameters. The accuracy of the Bayesian-optimized RF model will be significantly improved. Additionally, R_L is the random number list generated by the computer. It's only used as a reference for comparing the importance of the factors.

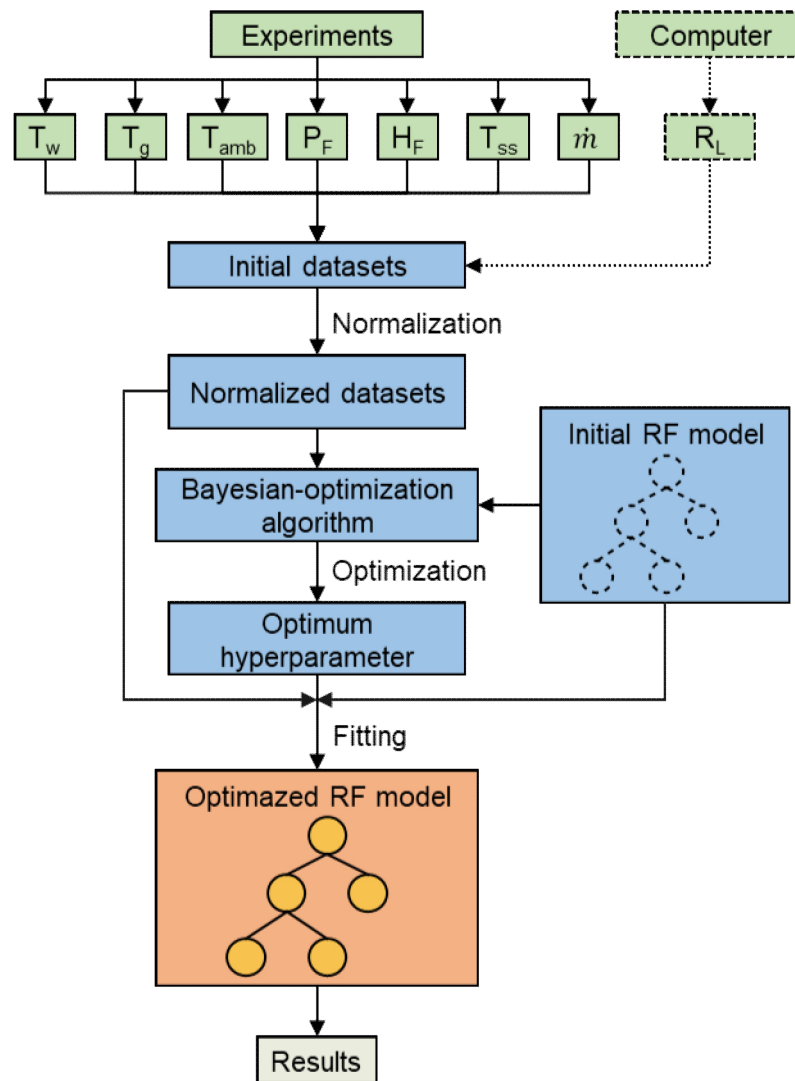


Fig.S2 The flow chart of using RF for predicting productivity and calculating the factor importance of the STD system.

3.2 BP-ANN

This work uses a five-layer perceptron with 3 hidden layers. When a training sample is inputted, the output error signal E_p of the model is

$$E_p = \frac{1}{2} (d_p - o_p)^2 \quad (\text{S14})$$

Where d and o are the predicting and true values; p is the label.

Based on the BP neural network algorithm, the model transmits the error signal back through the network, adjusts the weights between nodes, and the updated result is

$$w' = w + \Delta w = w - \frac{\partial E}{\partial w} \quad (\text{S15})$$

The activation function uses a unipolar Sigmoid function, and the weight adjustment is:

Output layer,

$$\begin{aligned} \Delta w_i^4 &= \eta \delta^4 y_i^3 = \eta (d - o) o (1 - o) y_i^3 \\ i &= 0, 1, \dots, m_3 \end{aligned} \quad (\text{S16})$$

Third hidden layer,

$$\begin{aligned} \Delta w_{ij}^3 &= \eta \delta_j^3 y_i^2 = \eta (\delta^4 w_j^4) y_j^3 (1 - y_j^3) y_i^2 \\ i &= 0, 1, 2, \dots, m_2 ; j = 1, 2, \dots, m_3 \end{aligned} \quad (\text{S17})$$

Second hidden layer,

$$\begin{aligned} \Delta w_{ij}^2 &= \eta \delta_j^2 y_i^1 = \eta \left(\sum_{a=1}^{m_3} \delta_a^3 w_{ja}^3 \right) y_j^2 (1 - y_j^2) y_i^1 \\ i &= 0, 1, 2, \dots, m_1 ; j = 1, 2, \dots, m_2 \end{aligned} \quad (\text{S18})$$

First hidden layer,

$$\begin{aligned} \Delta w_{ij}^1 &= \eta \delta_j^1 x_i = \eta \left(\sum_{a=1}^{m_2} \delta_a^2 w_{ja}^2 \right) y_j^1 (1 - y_j^1) x_i \\ i &= 0, 1, 2, \dots, k ; j = 1, 2, \dots, m_1 \end{aligned} \quad (\text{S19})$$

where w is the weight between the layer and the previous layer; y is the output of the neuron; m_1, m_2, m_3 are the numbers of neurons from the first hidden layer to the third hidden layer; k is the number of input parameters; $\eta \in (0,1)$ is the scale

coefficient, a larger value means a faster convergence speed but the local optimum may not be obtained, and a smaller value means higher accuracy and slower convergence speed. δ is the error signal between the neural network layer and the previous layer, the result can be calculated by reverse iteration, and the formula is,

$$\delta_j^h = \sum_{r=1}^{m_{h+1}} (\delta_r^{h+1} w_{jr}) y_j (1 - y_j), \quad j = 1, 2, \dots, m_h \quad (\text{S20})$$

The updated biase b' is

$$b' = b + \Delta b = b - \frac{\partial E}{\partial b}$$

The activation function uses a unipolar Sigmoid function, and the bias adjustment is:

Output layer,

$$\Delta b^3 = \eta \delta^4 = \eta (d - o) o (1 - o)$$

Third hidden layer,

$$\Delta b_j^2 = \eta \sum_j^{m_3} \delta_j^3 = \eta \sum_j^{m_3} (\delta^4 w_j^4) y_j^3 (1 - y_j^3) \\ j = 1, 2, \dots, m_3$$

Second hidden layer,

$$\Delta b_j^1 = \eta \sum_j^{m_2} \delta_j^2 = \eta \sum_j^{m_2} \left[\left(\sum_{a=1}^{m_3} \delta_a^3 w_{ja}^3 \right) y_j^2 (1 - y_j^2) \right] \\ j = 1, 2, \dots, m_2$$

First hidden layer,

$$\Delta b_j^0 = \eta \sum_j^{m_1} \delta_j^1 = \eta \sum_j^{m_1} \left[\left(\sum_{a=1}^{m_2} \delta_a^2 w_{ja}^2 \right) y_j^1 (1 - y_j^1) \right] \\ j = 1, 2, \dots, m_1$$

For the training set with a sample size of N, the root mean square error is used as the total error of the model,

$$E_{RME} = \sqrt{\frac{1}{N} \sum_{i=1}^N \left[\frac{1}{2} (d_i - o_i)^2 \right]} \quad (S21)$$

When $E_{RME} < E_{min}$ is satisfied or the maximum number of iterations is reached, the training ends and the artificial neural network prediction model is obtained. The forward pass prediction process is:

Firstly, from the input layer to the first hidden layer,

$$\alpha_h = AF \left[\sum_{i=1}^k (w_{ih}^1 x_i - b_h^0) \right] \quad h = 1, 2, \dots, m_1 \quad (S22)$$

where x_i is the input value; α_h is the value of the h_{th} neuron in the first hidden layer; AF is the activation function.

Secondly, from the first hidden layer to the second hidden layer,

$$\beta_h = AF \left[\sum_{i=1}^{m_1} (w_{ih}^2 x_i - b_h^1) \right] \quad h = 1, 2, \dots, m_2 \quad (S23)$$

where β_h is the value of the h_{th} neuron in the second hidden layer.

Then, from the second hidden layer to the third hidden layer,

$$\gamma_h = AF \left[\sum_{i=1}^{m_2} (w_{ih}^3 x_i - b_h^2) \right] \quad h = 1, 2, \dots, m_3 \quad (S24)$$

where γ_h is the value of the h_{th} neuron in the third hidden layer.

Lastly, from the third hidden layer to the output layer,

$$d = AF \left[\sum_{i=1}^{m_3} (w_i^3 x_i - b^3) \right] \quad (S25)$$

3.3 MLR

Multiple linear regression is obtained based on the least squares method. The multiple linear regression equation needs to satisfy the matrix equation.

$$\hat{y} = \hat{\beta}_0 + \hat{\beta}_1 x_1 + \hat{\beta}_2 x_2 + \dots + \hat{\beta}_k x_k \quad (S26)$$

$$X^T X \hat{B} = X^T Y \quad (S27)$$

where

$$Y = \begin{pmatrix} y_1 \\ y_2 \\ \vdots \\ y_N \end{pmatrix}, X = \begin{pmatrix} 1 & x_{1\ 1} & \cdots & x_{1\ k} \\ 1 & x_{2\ 1} & \cdots & x_{2\ k} \\ \vdots & \vdots & \ddots & \vdots \\ 1 & x_{N\ 1} & \cdots & x_{N\ k} \end{pmatrix}, \hat{B} = \begin{pmatrix} \hat{\beta}_0 \\ \hat{\beta}_1 \\ \vdots \\ \hat{\beta}_k \end{pmatrix} \quad (S28)$$

where y is the true value; x is the input value; β is the constant; N is the dataset number k is the number of the parameters.

The coefficient matrix can be obtained as,

$$\hat{B} = (X^T X)^{-1} X^T Y \quad (S29)$$

In this part, the Python library “sklearn.ensemble” is used in the RF model; “sklearn.neural_network” is used in the BP-ANN model; “sklearn.linear_model” is used in the MLR model.

Note S4、 The process of tuning hyperparameters by Bayesian optimization

The probability surrogate model (PSM) is based on Gaussian process regression (GPR). Gaussian processes have been widely used in regression, classification, and many fields that require inference of black-box models [2]. The data (X, Y) satisfies the Gaussian process,

$$Y = f(X) \sim N(\mu(X), K) \quad (S30)$$

where $f(X)$ is the gaussian process; $\mu(X)$ is the mean function; K is covariance function.

$$\mu(X) = [\bar{x}_1, \bar{x}_2, \cdots, \bar{x}_n] \quad (S31)$$

$$K = \begin{bmatrix} k(X_1, X_1) & k(X_1, X_2) & \cdots & k(X_1, X_t) \\ k(X_2, X_1) & k(X_2, X_2) & \cdots & k(X_2, X_t) \\ \vdots & \vdots & \ddots & \vdots \\ k(X_t, X_1) & k(X_t, X_2) & \cdots & k(X_t, X_t) \end{bmatrix} \quad (S32)$$

where n is the number of dimensions; t is the number of the data; $k(X_i, X_j)$ is the kernel function.

The kernel function in this work is Matern 2.5 kernel. It means that the Matern kernel function is a twice differentiable function,

$$k(X_i, X_j) = \frac{1}{\Gamma(\nu)2^{\nu-1}} \left(\frac{\sqrt{2\nu}}{l} d(X_i, X_j) \right)^\nu K_\nu \left(\frac{\sqrt{2\nu}}{l} d(X_i, X_j) \right) \quad (\text{S33})$$

where ν is a half-integer; l is the characteristic length-scale; $\Gamma_\nu(\nu)$ is the gamma function; $d(X_i, X_j)$ is the Euclidean distance; K_ν is a modified Bessel function. Abramowitz and Stegun^[3] gave a general solution. When ν is 2.5, it is,

$$k_{\nu=2.5}(X_i, X_j) = \left(1 + \frac{\sqrt{5} d(X_i, X_j)}{l} + \frac{5d(X_i, X_j)^2}{3l^2} \right) \exp \left(- \frac{\sqrt{5} d(X_i, X_j)}{l} \right) \quad (\text{S34})$$

For a new point (X^*, y^*) , it satisfies the joint Gaussian probability density function,

$$p(Y_{1:t}, y^*) = N \left(\begin{bmatrix} \mu(Y_{1:t}) \\ \mu(y^*) \end{bmatrix}, \begin{bmatrix} K & K^* \\ K^* & K^{**} \end{bmatrix} \right) \quad (\text{S35})$$

where $Y_{1:t}$ is the observed data. The covariance functions are,

$$\begin{aligned} K^* &= [k(X_1, X^*), k(X_2, X^*), \dots, k(X_t, X^*)] \\ K^{**} &= k(X^*, X^*) \end{aligned} \quad (\text{S36})$$

And then

$$\overline{y^*} = \mu(y^*) + K^* K^{-1} (Y_{1:t} - \mu(Y_{1:t})) \quad \text{var}(y^*) = K^{**} - K^* K^{-1} K^{*T} \quad (\text{S37})$$

However, in practical applications, it is very difficult to specify a clear and reasonable prior mean function^[2]. For simplicity, it is usually assumed that the prior mean function is a constant 0 function^[4].

$$\overline{y^*} = K^* K^{-1} Y_{1:t} \quad (\text{S38})$$

The posterior mean after data correction is not limited to 0, so this assumption has little effect on the posterior accuracy^[4].

The confidence bound strategy has been widely used in the field of K-arm gambling machines^[5], thus the acquisition function is based on the upper confidence bound (UCB).

$$\alpha_t(X^*; X_{1:t}) = \mu(X_{1:t}) + \sqrt{\beta_{1:t}} \sigma(X_{1:t}) \quad (\text{S39})$$

Where μ is the expectation value; σ is Variance; β is constant and balances expectation value and variance.

The Python library “bayes_opt” is used in this part. In this Python library, the characteristic length-scale l defaults to 1, and the $\sqrt{\beta}$ defaults to 2.576.

The hyperparameters of BP-ANN and RF are shown in Table S1 and Table S2.

Table S1 The hyperparameter of BP-ANN (The detailed functions can refer to the official website of `sklearn.neural_network.MLPRegressor`)

Hyperparameter	Optimization Range	Function
hidden_layer_sizes	first (h_1)	Generate the construction of the hidden layer in BP-ANN
	second (h_2)	
	third (h_3)	
activation (h_4)	['identity', 'logistic', 'tanh', 'relu']	Activation function for the hidden layer.
solver (h_5)	['lbfgs', 'sgd', 'adam', 'sgd']	The solver for weight optimization.

Table S2 The hyperparameter of RF (The detailed functions can refer to the official website of `sklearn.ensemble.RandomForestRegressor`.)

Hyperparameter	Optimization Range	Function
n_estimators (h_1)	(1, 200)	The number of trees in the forest
min_samples_split (h_2)	(2, 8)	The minimum number of samples required to split an internal node
max_features (h_3)	(0.01, 0.999)	The number of features to consider when looking for the best split
max_depth (h_4)	(20, 60)	The maximum depth of the tree.
criterion (h_5)	['mae', 'mse']	The function to measure the quality of a split

Note S5、 K-fold cross-validation

Splitting the data set by K-fold cross-validation makes full use of each data to test. It improves the overall stability of the model. The 5-fold cross-validation (20% testing set) is used in this part, which is in keeping with the “Method of splitting the data set”. The schematic diagram of the 5-fold cross-validation is shown in Fig. S3. In the first fitting process, the first fold data is used as the test set, and the other data is used as the training set to fit the model. It obtains the first set of evaluation indicators. In the second fitting process, the second fold data is used as the test set, and the other data is used as the training set to fit the model to obtain the second set of evaluation indicators. Until the fifth time, all 5-fold data were used as the test set, and five sets of evaluation indicators were obtained. After taking the average value, the model evaluation index of a 5-fold cross-validation was obtained. The Python library “sklearn.model_selection” is used in this part.

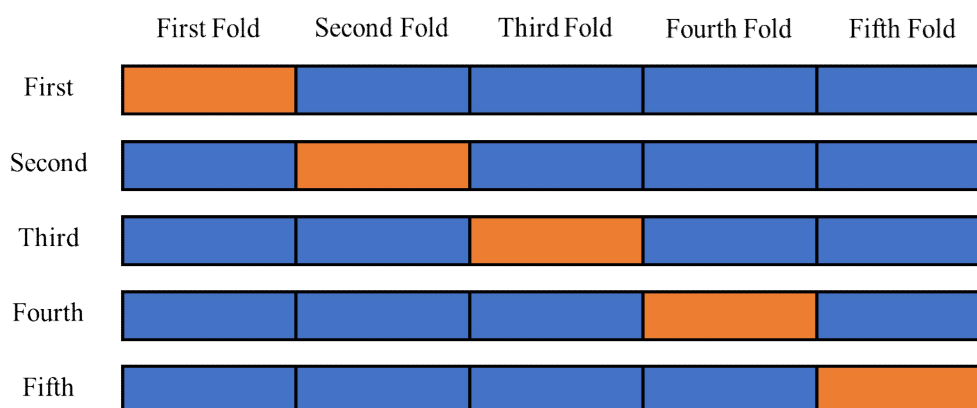


Fig. S3 The schematic of 5-fold cross-validation: the blue/oranges are training/test sets

Note S6、 The process of testing model

Based on the five-fold cross-validation and the Bayesian optimization, the RF model and BP-ANN model are trained and built by the optimized hyperparameters. To avoid the occasionality of the results, the process of the above modeling is repeated ten times, and the evaluation indexes and errors of the models are obtained by calculating the mean and standard deviation.

Note S7、 Other instructions

In addition to the Python libraries mentioned above, Table S3 shows the other Python libraries used in this work and their functions.

Table S3 The other Python libraries

Name	Functions
random	Random number module
Matplotlib	Plot figure
numpy	Store and process large multidimensional matrices
pandas	Import files

Note S8、 Effect of dataset range of P_F

The effect of the data ergodicity from the aspect of P_F is shown in Fig. S4. Two different ranges of P_F are analyzed and compared, i.e., 0 – 0.3 W and 0 – 0.9 W. The data size of the two different ranges is the same, which is around 500 data. According to the experimental results, the productivity enhancement due to the fan mostly contributes to the range of 0 – 0.3 W. The productivity is almost constant in the range of 0.3 – 0.9 W in most cases. The results show that in the range of 0 – 0.3 W, T_w and T_g are the most important two factors, followed by T_{amb} , P_F , and T_{ss} . H_F and R_L are the least important factors. The same rank happens in the range of 0 – 0.9 W, which indicates that the convergence range doesn't cover up or mislead the importance of the factors. Therefore, it might be concluded that measuring as much data as possible doesn't have a significant negative effect on the analysis of factor importance.

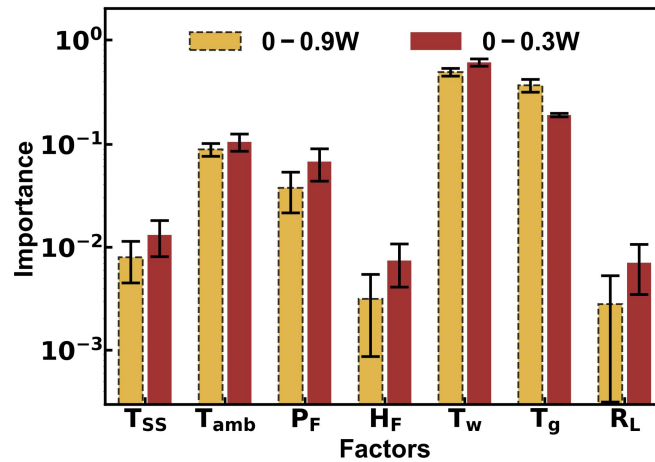


Fig. S4 Effect of data range of P_F .

References

- [1] Boobier S, Hose D R, Blacker A J, et al. Machine learning with physicochemical relationships: solubility prediction in organic solvents and water [J]. Nature Communications, 2020, 11(1): 1-10.
- [2] Williams C K, Rasmussen C E. Gaussian processes for machine learning [M]. MIT press Cambridge, MA, 2006.
- [3] Florentin J. Handbook of Mathematical Functions [M]. JSTOR. 1966.
- [4] Cui J, Yang B. Survey on Bayesian optimization methodology and applications [J]. Journal of Software, 2018, 29(10): 3068-3090.
- [5] Lai T L, Robbins H. Asymptotically efficient adaptive allocation rules [J]. Advances in Applied Mathematics, 1985, 6(1): 4-22.